ADVANCED FUNCTIONAL MATERIALS
www.afm-journal.de

Bandgap Engineering in OH-Functionalized Silicon Nanocrystals: Interplay between Surface Functionalization and Quantum Confinement

Marius Bürkle, Mickaël Lozac'h, Calum McDonald, Davide Mariotti, Koji Matsubara, and Vladimir Švrček*

In this work, a systematic first-principles study of the quasi-band structure of silicon nanocrystals (Si-NCs) is provided, focusing on bandgap engineering by combining quantum confinement of the electronic states with OH surface-functionalization. A mapping between the bandgap, Si-NC diameter, and the degree of hydroxide coverage is provided, which can be used as a guideline for bandgap engineering. Complementary to first-principles calculations, the photoluminescence (PL) wavelength of Si-NCs in the quantum-confinement regime is measured with well-defined diameters between 1 and 4 nm. The Si-NCs are prepared by means of a microplasma technique, which allows a surfactant-free engineering of the Si-NCs surface with OH groups. The microplasma treatment technique allows us to gradually change the degree of OH coverage, enabling us, in turn, to gradually shift the emitted light in the PL spectra by up to 100 nm to longer wavelengths. The first-principles calculations are consistent with the experimentally observed dependence of the wavelengths on the OH coverage and show that the PL redshift is determined by the charge transfer between the Si-NC and the functional groups, while on the other hand surface strain plays only a minor part.

1. Introduction

Silicon (Si) is one of the most abundant elements on Earth and indispensable in the microelectronic and photovoltaic industry. However, bulk Si is an in direct bandgap semiconductor, which limits its applicability, e.g., in light-emitting devices and high-efficiency third-generation solar cells. Unlike bulk Si, small particles of silicon, about a few nanometers in size, allow energy bandgap tuning by the quantum confinement effect that gives luminescent properties at room temperature with a photoluminescent quantum yield of up to 60–75%.[1] The exciton Bohr radius for silicon was estimated to be merely 4.2 nm,[2] which brings another important feature at nanometer size: the large surface to bulk ratio. It has been established that both the quantum confinement and a defined functionalization of the silicon nanocrystal (Si-NC) surface and the control of the surface chemistry is crucial for tailoring the optical properties of Si-NCs.[3–7] Obviously, the impact of surface functionalization is more significant for nanocrystals below 4 nm with strong quantum confinement of electrons and holes. The interplay of quantum confinement effect and surface functionalization might even lead to a change of the nature of the bandgap from indirect to direct.[6,8–11] The challenge is how to effectively modify the surface of Si-NCs at quantum confinement size without disturbing the transport within the Si-NCs. Hydride terminated Si-NCs are widely studied since they are available at high purities allowing good photoluminescent properties.[12–15] However, the surface functionalization is only possible using alkenes and alkynes via hydrosilylation, which limits the functional groups that can be bound on the Si-NC's surface.[12,13] Due to these limitations, mostly alkyl chains are currently used to stabilize the Si-NC's surface against oxidation. This treatment forms an insulating layer on the Si-NC's surface, which possibly hampers their applicability in, e.g., solar cells.[16] In this sense, the use of atmospheric pressure plasmas for the surface treatment of Si-NCs prepared by electrochemical etching is advantageous[9,17] as it allows a surfactant-free fabrication of Si-NCs, that is, it largely avoids contamination of the NC surface by active agents (i.e., surfactants)[18] that are normally present on the NC surface when prepared, for instance, by chemical synthesis from precursors.[19] Thus, the microplasma capability of coupling plasmas with Si-NCs in colloids provides a complementary approach to traditional wet chemistry,[19] and is especially attractive as it allows: i) ease storage, ii) processing via low-cost techniques such as screen printing, and iii) to supply and use the Si-NCs in liquids, for example, when intended for medical applications.[20]

In recent years we have developed and studied atmospheric plasmas induced surface engineering of Si-NCs prepared by

Dr. M. Bürkle, Dr. M. Lozac'h, Dr. K. Matsubara, Dr. V. Švrček
National Institute of Advanced Industrial Science and Technology (AIST)
Central 2, Umezono 1-1-1, Tsukuba 305-8568, Japan
E-mail: marius.buerkle@aist.go.jp
Dr. C. McDonald, Prof. D. Mariotti
Nanotechnology and Integrated Bioengineering Centre (NIBEC)
University of Ulster
Newtownabbey BT37 0QB, UK
The ORCID identification number(s) for the author(s) of this article can be found under https://doi.org/10.1002/adfm.201701898.

DOI: 10.1002/adfm.201701898

electrochemical etching from high-quality wafers,[9,21] which allows us to fabricate surfactant-free and well-defined Si-NCs with sizes within the quantum confinement regime and to functionalize the Si-NC surface with OH groups. The high crystalline quality, which is not perturbed by the atmospheric plasma treatment,[9,22,23] and good definition of the Si-NCs before and after atmospheric plasma treatments have been confirmed by high-resolution transmission electron microscopy (HRTEM) and Raman.[22,23] Furthermore, surface characterization by means of X-ray photoelectron spectroscopy (XPS)[24] and Fourier transform infrared spectroscopy (FTIR)[17,22] clearly shows that our atmospheric-plasma-based approach mostly acts on the NC surface,[9] and the surface chemistry after the plasma treatments was quantified by means of FTIR, confirming the OH functionalization.[22,24]

To engineer the bandgaps and optical properties of tailored Si-NCs a precise control of both, the size and the surface chemistry, is necessary. It has been shown experimentally and theoretically that replacement of H-terminations with oxygen-based terminations such as Si-OH or Si-O-R (i.e., including radicals) in Si-NCs produces a consistent shift toward longer wavelengths (the so-called redshift) in the photoluminescence (PL) spectra and an enhanced PL quantum yield.[24,25] In this study we take advantage of the possibility to gradually change the OH coverage of Si-NCs with well-defined sizes in the quantum confinement regime using the microplasma at atmospheric pressure, as outlined above, where the atmospheric microplasma was generated between a nickel tubing and the surface of the ethanol-Si-NCs colloidal dispersion, whereby a carbon rod held at positive voltage was used as counter electrode while the nickel tubing was connected to the ground. We observe a gradual shift of the emitted light in the photoluminescence spectra by around 100 nm to longer wavelengths. Previous theoretical studies already suggested that varying Si-NC size and OH functionalization can lead to a redshift of the PL spectra due to charge redistribution at the Si-NC surface,[3,4] however, these studies focus on small clusters with a single OH group; a systematic study addressing the coverage dependence of realistic-sized systems has yet to be provided. In this work we therefore consider by means of first-principles calculations both Si-NC crystals with sizes corresponding to the diameters present in experiment and gradually varying OH coverage. This allows us to elucidate the origin of experimentally observed redshift in a systematic way. We show that the redshift is mainly caused by charge redistribution at the Si-NC surface and only to a minor extent by mechanical strain. Based on our systematic study we provide a simple guide line for bandstructure engineering with respect to an optimal combination of quantum confinement, i.e., particle size, and surface functionalization.

2. Results and Discussion

First, we analyze the size of the Si-NC studied in this work. The Si-NCs diameter is a critical feature that directly influences the bandgap of the Si-NCs and can determine the outcome of the OH functionalization through the microplasma processing technique. The size distribution of the Si-NCs after the DC microplasma processing is obtained from transmission electron microscope (TEM) analysis[26] and given in **Figure 1**. Our Si-NCs show a narrow size distribution with diameters between 1 nm to 6 nm. The average diameter of the optical active Si-NCs, due to quantum confinement,[3,27,28] is given by ≈2.3 nm and narrowly peaked between 1 nm and 4 nm. In the next step we functionalize the Si-NC surface. During the microplasma processing the Si-NCs gradually acquire oxygen-based termination, including, with a vary degree of coverage, Si-OH groups.[9,17] The PL spectra of the surface engineered Si-NCs shifts thereby to longer wavelengths as a function of the processing time, i.e., with increasing OH coverage. The shift of the PL spectra saturates after ≈80 min of processing time at 0.22 ± 0.02 eV which corresponds to a wavelength shift of around 100 nm from 590 to 690 nm (Figure 3a). Where it has to be noted that the experimentally observed PL shift is the average over the particle size of the optical active Si-NCs as it is not possible in experiment to resolve the PL shift individually for each particle size present. To relate the average PL shift to the OH coverage, i.e., number of OH units on the Si-NC surface, we assume a Langmuir-like adsorption rate[29] $n_{OH}(t) = n_{max}(1 - e^{-\lambda t})$ which allows us to express the shift $\sigma(t) = \sigma^0 - \gamma n_{OH}(t)$ of the initial PL maxima $\sigma(t = 0) = \sigma^0$ in terms of the processing time as

$$\sigma(t) = \sigma^0 - \delta\left(1 - e^{-\lambda t}\right), \quad (1)$$

where we combined the maximum OH coverage n_{max} with the average substituent shift per OH unit γ to $\delta = \gamma n_{max}$ and assume a time independent adsorption rate $\lambda > 0$. While Equation (1) only takes the substituent induced PL shift into account, neglecting, e.g., inhomogeneous surface reconstruction, different kind of adsorbates, varying surface to volume ratio, it reproduces the observed time dependence closely (Figure 3b) suggesting that the observed shift is indeed mainly caused by one well-defined functional group and that for the particle size present the adsorption remains comparable. Moreover, it is worth noting that the relative PL shift is almost complete with an OH coverage between 75% and 90% (Figure 3c).

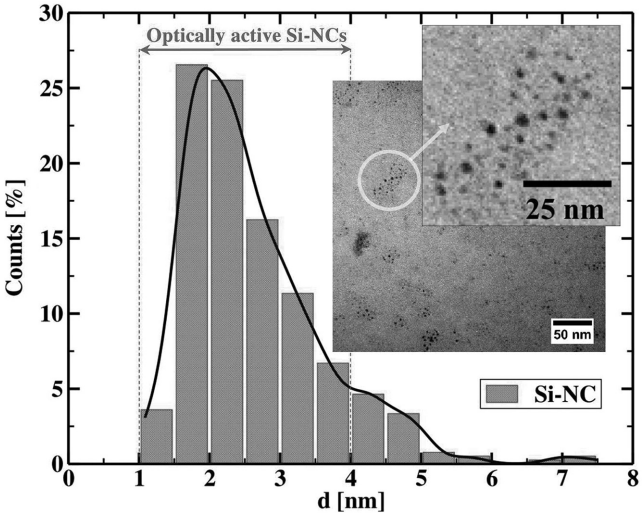

Figure 1. Size distribution of the Si-NCs obtained from TEM analysis. TEM images (inset): Reproduced with permission.[24] Copyright 2013, Wiley-VCH.

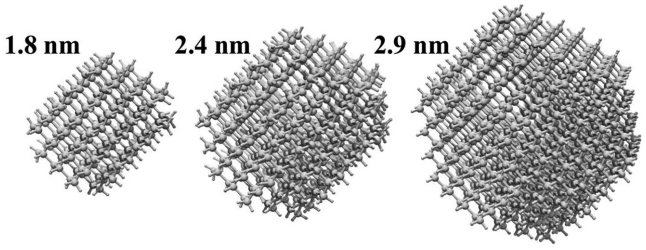

Figure 2. Si-NCs considered in the DFT calculations, here shown with hydrogen passivation.

To elucidate the origin of the PL shift we performed density functional theory (DFT) calculations of the quasi band structure[30,31] for Si-NCs with diameters of 1.8, 2.4, and 2.9 nm (**Figure 2**), and gradually increasing OH coverage from 0% to 100% (by 25% steps) by successively replacing randomly selected hydrogen atoms with OH in each step. Where it is worth noting that there are no energetically preferable binding sites for OH and only small variations of the charge transfer with respect to the actual OH binding position (see Supporting Information). The corresponding quasi band structure for OH coverage of 0%, 50%, and 100% is summarized in Figure 4a, where we have taken the thermal broadening of the levels into account, which leads to the formation of quasi continuous bands at room temperature (T = 300 K), especially it tends to smear out minigaps, which are known to affect the relaxation of hot electrons.[31] Where it has to be noted that, due to the lack of translational symmetry, points in different Brillouin zones (BZ) are not equivalent,[31] here we plot the quasi-band structure from Γ_0 in the first BZ to X and then Γ_1 in an adjacent BZ. In the following we focus on the transition between the conductance band edge at the X-point and the valence band edge at Γ_1, which is consistent with the experimentally observed indirect bandgap. For the smallest cluster, d = 1.8 nm, with 100% OH an additional transition can occur between Γ_0 and Γ_1, which can however expected to be suppressed as Γ_0 and Γ_1 are located in different BZs and corresponding signatures were not observed in experiment. The dependence of the bandgap on the Si-NC diameter and OH coverage is summarized in Figure 4b. Comparing the calculated bandgaps directly with experiment is, however, difficult due to the well-known deficiency of approximate DFT to quantitatively predict the bandgaps of semiconductors[32] and due to the size distribution of the Si-NC diameters present in experiment resulting in an size-average PL shift. Moreover, it has been shown that corrections introduced by time dependent methods are minimal in Si-NCs based systems[33] and that the one-particle picture is able to capture the essential electronic properties correctly due an approximate cancelation of self-energy and Coulomb corrections.[33–35] Therefore, the relative PL shift $\sigma(t)/\sigma^0$ between the pristine Si-NCs with hydrogen termination (σ^0) and the ones with increasing OH coverage ($\sigma(t)$) can be expected to be well reproduced by our static DFT picture and to be approximately independent of the actual diameter of the Si-NCs studied here. As shown in **Figure 3**c, the calculated relative PL shifts for all three Si-NC diameters follows the experimentally observed trend and are consistent with the assumed Langmuir-like time dependence of the OH coverage and remains roughly independent of the particle size, supporting the assumption made above that the adsorption rate is in first-order indeed independent of the particle size. An exception is the smallest Si-NC (d = 1.8 nm) with large OH coverage (75% and 100%) where the calculated relative PL shifts are larger than what we observe in experiment, which is mainly related to diffuse states at the band edges caused by the strong interplay between quantum confinement and surface functionalization.

For 0% of OH coverage we observe with decreasing Si-NC size a bandgap opening[36,37] of around 0.6 eV (**Figure 4**b). Conversely, increasing the OH coverage leads to a reduction of the bandgap. The effect of surface engineering with OH is more pronounced for the smallest clusters (d = 1.8 nm). Essentially both important effects present at nanoscale: the quantum confinement effect which leads to a bandgap opening and the influence of surface functionalization which allows to a decrease the bandgap can be clearly observed here. To tune the optical properties at nanoscale by means of bandgap engineering both effects must be taken into account. The possible range of suitable combinations of size and OH coverage for bandgap engineering are indicated by A and B. In A the bandgap opening

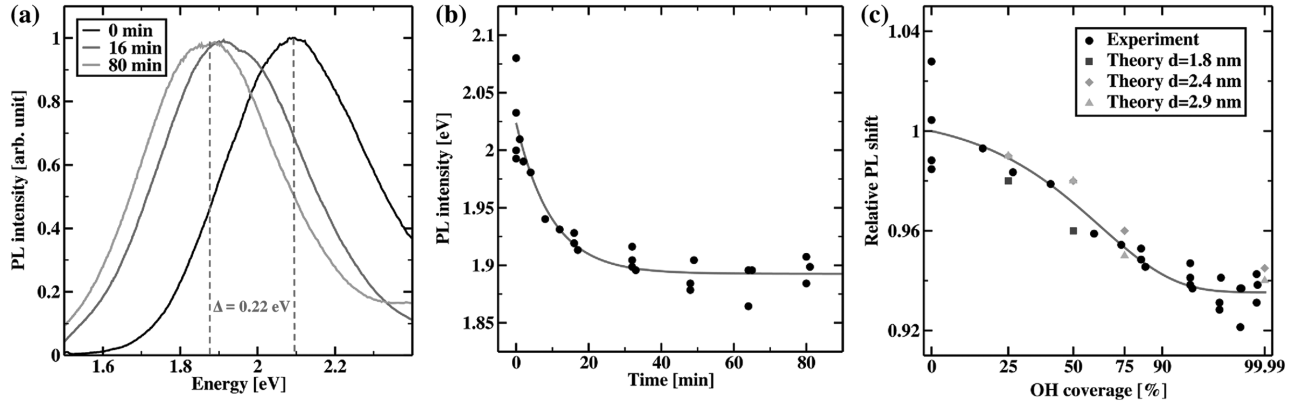

Figure 3. a) Measured PL shift for pristine Si-NCs (t = 0 min, right-hand line) and after t = 16 min (middle line) and t = 80 min (left-hand line) processing times. b) Measured PL intensities fitted into Equation (1) assuming a Langmuir-like time dependence (solid line). c) Relative PL shifts obtained from theory, experiment, and Equation (1) fitted into the experimental results (solid line). For the calculated Si-NCs with d = 1.8 nm, the data points at 75% and 100% OH coverage have been omitted as they do not follow the observed dependence.

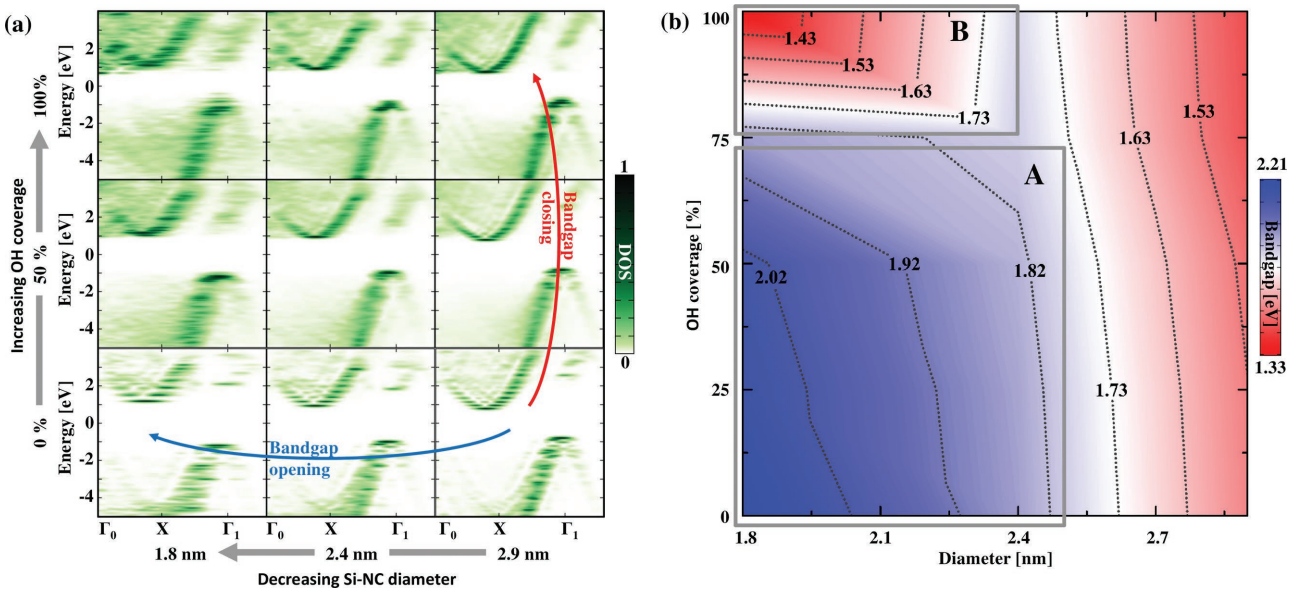

Figure 4. a) Quasi-band structure obtained from DFT calculations for 0%, 50%, and 100% OH coverage (for brevity 25% and 75% have been omitted), where the energy origin has been set into mid gap. b) Dependence of the calculated bandgap on the Si-NC diameter and OH coverage, where the bandgap is represented by the contour color. The two regions favorable for bandgap engineering are marked A and B.

effect dominates over the OH coverage induced effects for coverage below 60%. Area B indicates the bandgap decreasing that is triggered for OH coverage above 75% and is also more pronounced at smaller cluster size due to the large surface to volume ratio.

After giving the quantitative discussion of the PL shift we want to rationalize its origin. Essentially the OH groups will give rise to i) a substituent related shift of the orbital energies due to charge transfer between the OH groups and the Si-NCs, and ii) strain induced by atomic rearrangement at the Si-NCs surface. For methyl-passivated silicon nanocrystals it has been suggested that the latter effects can lead to large variations of the optical properties,[6] for the polar OH groups it is on the other hand reasonable to assume that the former effect may play a decisive role. To quantify both effects we calculated the charge distribution on the Si-NC[38] (**Figure 5**a) and the absolute strain relative to the bulk Si-Si distance (Figure 5b), both averaged over nearest neighbor shells. First, we consider the effect of the charge transfer between the Si-NC and the functional groups. The charge redistribution mainly occurs at the outermost three layers of the Si-NC. On the outermost shell electrons are depleted, while on the next inner shell partial negative charge is accumulated. With increasing OH coverage, i.e., increasing charge transfer, the partial positive charge on the outermost shell increases significantly, while the inner shells remain on average neutral. Accordingly we observe a large increase of the absolute dipole moment $|p|$, which is approximately vanishing for the pristine Si-NCs with hydrogen passivation and $|p|_{d\,=\,1.8\,\mathrm{nm}} \approx 50\,\mathrm{D}$, $|p|_{d\,=\,2.4\,\mathrm{nm}} \approx 12\,\mathrm{D}$, and $|p|_{d\,=\,2.9\,\mathrm{nm}} \approx 39\,\mathrm{D}$ for 100% OH. The charge transfer decreases the energy of both the conductance and valence states; however, the shift Δ_c for the conduction band-like unoccupied states is larger than the shift Δ_v for the valence band-like occupied levels leading to the overall decrease of the bandgap with increasing OH coverage (Figure 5c). Next, we want to discuss the effects of the induced strain. Essentially, the average absolute strain remains small and does not exceed 1.1% for the outermost two shells and decreases rapidly for the inner shells where the lattice is only weakly perturbed (Figure 5b). In order to separate the effects of the strain from the substituent induced effects we adopt the following model. For the Si-NC with $d = 2.9\,\mathrm{nm}$ we take the atomic positions of Si from the fully relaxed structure with 100% OH coverage but we replace the OH groups with hydrogen. For this Si-NC we relax the atomic positions of the hydrogen atoms but we keep the Si atoms fixed, i.e., we impose strain similar to the fully OH covered Si-NC. The corresponding band structure of the Si-NC with imposed strain as well as the band structure of the Si-NC without imposed strain, i.e., the fully relaxed pristine Si-NC with H passivation, is given in Figure 5d. Essentially, the imposed strain leads to a slightly increased k-space delocalization due to the perturbation of the Si lattice and only to minor level shift which is essentially negligible compared to the previously discussed substituent shift. Thus, for the OH-functionalized Si-NCs studied here the change of the optical properties is induced by the changes of the surface electronic structure caused by charge transfer between the polar OH groups and the Si-NC rather than by mechanical strain.

3. Conclusion

To summarize, for silicon nanocrystals in the quantum confinement regime we showed that functionalizing the surface of initially hydrogen passivated nanocrystals with OH groups leads to an substantial redshift in the photoluminescence spectra of 0.22 ± 0.02 eV corresponding to a shift to longer wavelength of around 100 nm. The experimental observations are rationalized by systematic study of the size and coverage dependence

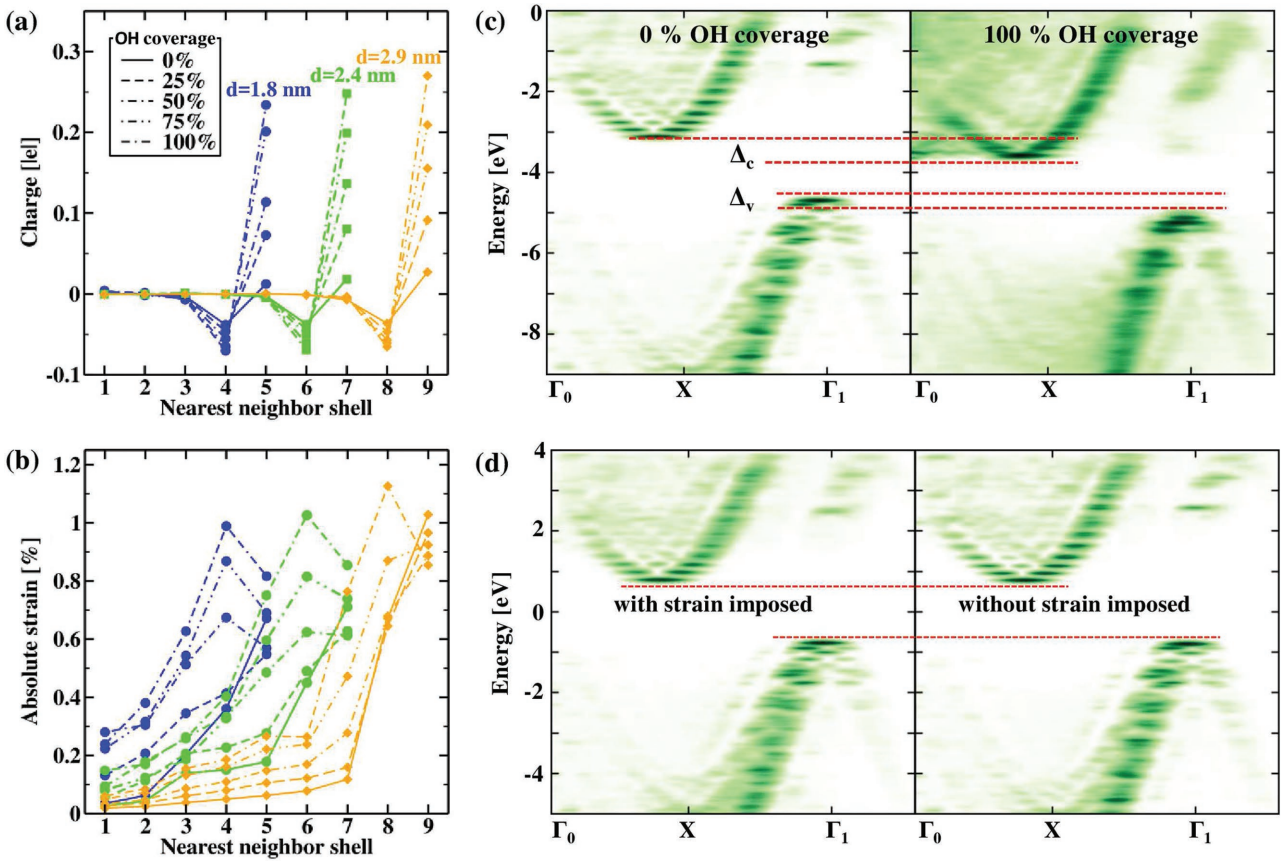

Figure 5. a) Charge and b) absolute strain averaged over nearest neighbor Si shells, where the innermost shell is denoted by 1. c) Absolute movement of the bands for $d = 2.9$ nm with 0% and 100% OH coverage. d) Quasi-band structure for the Si-NC with $d = 2.9$ nm and hydrogen passivation without and with imposed external strain similar to 100% OH coverage.

of the bandgap using density functional theory calculations which reproduce the observed relative PL shift well. Our calculations show that essentially the effect of the OH groups is twofold; they give rise to charge transfer and redistribution at the outermost silicon shells of the nanocrystals, and they lead to strain induced by atomic rearrangement of the surface atoms. Based on these findings we conclude that for the OH groups studied here, the former effect dominates and the experimentally observed shift of the photoluminescence spectra mainly originates in substituent related effects and that the mechanical strain only plays a subordinate role. Our calculations emphasis the favorable domains for bandgap engineering at nanoscale. Where it is important to stress that with the approach presented in this work it is possible to gradually tune the optical properties over a wide range by suitable combinations of Si-NC diameter and OH coverage.

4. Experimental Section

Preparation of Functionalized Nanocrystals: Surface engineering by DC microplasma setup was used as reported elsewhere.[17] A powder containing only Si-NCs was produced by electrochemical etching of a silicon wafer and subsequent mechanical pulverization.[17] In particular, 5 mg of the Si-NCs powder was dispersed in 20 mL of ethanol. In order to remove the largest aggregates, the dispersion was left to settle for 15 min and the supernatant part has been used to produce a 10 mL sample of the ethanol-Si-NC's colloidal dispersion. The microplasma was generated between a nickel (Ni) tubing (inner diameter 0.7 mm and outer diameter 1 mm) and the surface of the ethanol-Si-NCs colloidal dispersion. As a counter electrode, a carbon rod of 5 mm diameter is immersed in the colloidal solution at a distance of about 3 cm from the Ni tubing. A positive voltage was applied to the carbon rod while the nickel tubing was connected to the ground through a 100 k Ohm resistor. Pure argon was flown inside the Ni tubing at a rate of 25 sccm (sccm denotes standard cubic centimeter per minute). The applied voltage was about 2 kV and current about 1.5 mA.

Estimation of the Size Distribution: The size distribution was obtained by computational treatment (thresholding) using the free software ImageJ[26] from the TEM image given in the inset of Figure 1. Due to the different light background intensity, the size distribution was estimated on four distinct areas and Figure 1 represents the sum of those four areas. A total of 422 particles on a surface of 110 958.4 nm^2 were analyzed.

First-Principles Calculations: The electronic and geometrical properties of the Si-NCs were obtained within density functional theory at the PBE level of theory[39,40] using the LANL2DZdp basis set[41,42] with polarization functions for all nonhydrogen atoms, namely, Si[43] and O.[44,45] The total energy calculations were converged with a precision of 10^{-7} a.u. All Si-NCs were fully relaxed and the structure optimization was carried out until the maximum norm of the gradient dropped below 1×10^{-5} a.u. The tight convergence criteria ensured well-converged electronic and geometrical structures. All calculations were carried out using the quantum chemistry package TURBOMOLE.[46] To ensure the robustness of the results, especially the charge transfer, obtained

using the pure DFT functional (PBE), the calculated charge transfer was checked against results obtained at the PBE0[47,48] level of theory. The differences, however, were found to be only very minor (see the Supporting Information).

Quasi-Band Structure: For finite-sized systems with broken translational symmetry, standard band structure theory could not be applied; an approximate band structure for finite-sized objects, such as the nanocrystals studies here, could be obtained by considering the *k*-space resolved density of states (DOS) for each molecular orbital.[6,30,31] Here, a Green's function technique was used to calculate the DOS where the thermal broadening of the discrete energy eigenstates was taken into account which led eventually to the formation of quasi-continuous bands in the finite-sized NCs. To calculate the *k*-space DOS, the spectral representation of the retarded Green's function was used

$$\hat{G}(E)=\sum_{\mu}\frac{|\mu\rangle\langle\mu|}{E+\mathrm{i}\eta-\varepsilon_{\mu}}, \tag{2}$$

where $|\mu\rangle$ is the energy eigenstate of the Hamiltonian $\hat{H}$ to the eigenvalue ε_{μ} and $\eta > 0$ an infinitesimal quantity. Here η could be kept finite, as a phenomenological parameter accounting for the broadening of the energy eigenstates; however, as the thermal broadening of the DOS was taken explicitly into account, this would not be necessary. The Green's function was related to the (local) DOS by $\rho_{\mu}(E)=-\frac{1}{\pi}\mathrm{Im}[G_{\mu\mu}(E)]$. To obtain the *k*-space information, ref. [31] was followed and the real space functions $\phi_{\mu}(\boldsymbol{r})=\langle \boldsymbol{r}|\mu\rangle$ were projected onto plane waves $\phi_{\mu}(\boldsymbol{k})=\int \mathrm{d}\boldsymbol{k}\langle \boldsymbol{r}|\boldsymbol{k}\rangle\langle \boldsymbol{k}|\mu\rangle=\int \mathrm{d}\boldsymbol{k}\mathrm{e}^{\mathrm{i}\boldsymbol{k}\boldsymbol{r}}\phi_{\mu}(\boldsymbol{r})$. With this, Equation (2) could be written for a selected MO μ in terms of $\phi_{\mu}(\boldsymbol{r})$

$$G(E,\varepsilon_{\mu};\boldsymbol{k})=\frac{\phi_{\mu}^{*}(\boldsymbol{k})\phi_{\mu}(\boldsymbol{k})}{E+\mathrm{i}\eta-\varepsilon_{\mu}}, \tag{3}$$

and the *k*-space resolved density of states for MO μ at temperature $T = 0$ K could be expressed as

$$\rho(E,\varepsilon_{\mu};\boldsymbol{k})=-\frac{1}{\pi}\mathrm{Im}\left[G\left(E,\varepsilon_{\mu};\boldsymbol{k}\right)\right] \tag{4}$$

where nondiagonal terms in *k*-space arising due to the broken translational symmetry were neglected.[49] For finite temperatures, the energy-dependent *k*-space resolved DOS at temperature T is given as the convolution of the negative energy derivative of the Fermi function $f'(E-E_1, T) = -\partial f(E-E_1, T)/\partial E$ with the DOS at $T = 0$ K

$$N(E,T;\boldsymbol{k})=\sum_{\mu}\int_{-\infty}^{\infty}\mathrm{d}E_1\rho(E,\varepsilon_{\mu};\boldsymbol{k})\times f'(E-E_1,T), \tag{5}$$

which follows directly from the definitions of the electron density $n(E,T)=\int_{-\infty}^{\infty}\mathrm{d}E_1\rho(E_1)f(E_1-E,T)$ and thermodynamic density of states $N(E, T) = \partial n(E, T)/\partial E$ at a given temperature T.

Supporting Information

Supporting Information is available from the Wiley Online Library or from the author.

Acknowledgements

This work was supported by Grant-in-Aid for Young Scientists (Start-up) (KAKENHI #15H06889) from Japan Society for the Promotion of Science and by the NEDO grant on Innovative Solar Cells and grant-in-aids for Scientific Research from the Japan Society of the Promotion of Science (JSPS, no. 25·03716). We thank the Engineering and Physical Sciences Research Council (EPSRC) for funding (EP/K022237/1, EP/M024938/1). The Acknowledgements section was updated on October 5, 2017, following initial online publication.

Conflict of Interest

The authors declare no conflict of interest.

Keywords

bandgap engineering, DFT calculations, photoluminescence measurements, silicon nanocrystals, solar cells

Received: April 10, 2017
Revised: June 22, 2017
Published online: August 2, 2017

[1] Q. Li, Y. He, J. Chang, L. Wang, H. Chen, Y.-W. Tan, H. Wang, Z. Shao, *J. Am. Chem. Soc.* **2013**, *135*, 14924.
[2] A. D. Yoffe, *Adv. Phys.* **1993**, *42*, 173.
[3] M. V. Wolkin, J. Jorne, P. M. Fauchet, G. Allan, C. Delerue, *Phys. Rev. Lett.* **1999**, *82*, 197.
[4] A. Puzder, A. J. Williamson, J. C. Grossman, G. Galli, *Phys. Rev. Lett.* **2002**, *88*, 097401.
[5] X. Li, Y. He, M. T. Swihart, *Langmuir* **2004**, *20*, 4720.
[6] K. Kůsová, P. Hapala, J. Valenta, P. Jelínek, O. Cibulka, L. Ondič, I. Pelant, *Adv. Mater. Interfaces* **2014**, *1*, 1300042.
[7] M. Dasog, K. Bader, J. G. C. Veinot, *Chem. Mater.* **2015**, *27*, 1153.
[8] K. Dohnalová, A. N. Poddubny, A. A. Prokofiev, W. D. de Boer, C. P. Umesh, J. Mj Paulusse, H. Zuilhof, T. Gregorkiewicz, *Light: Sci. Appl.* **2013**, *2*, e47.
[9] D. Mariotti, S. Mitra, V. Švrček, *Nanoscale* **2013**, *5*, 1385.
[10] B. G. Lee, J.-W. Luo, N. R. Neale, M. C. Beard, D. Hiller, M. Zacharias, P. Stradins, A. Zunger, *Nano Lett.* **2016**, *16*, 1583.
[11] I. Marri, M. Govoni, S. Ossicini, *Sol. Energy Mater. Sol. Cells* **2016**, *145*, 162.
[12] C. M. Hessel, D. Reid, M. G. Panthani, M. R. Rasch, B. W. Goodfellow, J. Wei, H. Fujii, V. Akhavan, B. A. Korgel, *Chem. Mater.* **2012**, *24*, 393.
[13] M. L. Mastronardi, F. Maier-Flaig, D. Faulkner, E. J. Henderson, C. Kübel, U. Lemmer, G. A. Ozin, *Nano Lett.* **2012**, *12*, 337.
[14] O. Wolf, M. Dasog, Z. Yang, I. Balberg, J. G. C. Veinot, O. Millo, *Nano Lett.* **2013**, *13*, 2516.
[15] K. Kůsová, O. Cibulka, K. Dohnalová, I. Pelant, J. Valenta, A. Fůcíková, K. Žídek, J. Lang, J. Englich, P. Matějka, P. Štěpánek, S. Bakardjieva, *ACS Nano* **2010**, *4*, 4495.
[16] C. Y. Liu, U. R. Kortshagen, *Nanoscale Res. Lett.* **2010**, *5*, 1253.
[17] V. Švrček, D. Mariotti, M. Kondo, *Appl. Phys. Lett.* **2010**, *97*, 161502.
[18] S. C. Mitchell, R. H. Waring, *Ullmann's Encyclopedia of Industrial Chemistry*, Wiley-VCH, Weinheim, Germany **2000**.
[19] I. M. D. Höhlein, A. Angi, R. Sinelnikov, J. G. C. Veinot, B. Rieger, *Chem. – Eur. J.* **2015**, *21*, 2755.
[20] S. Chinnathambi, S. Chen, S. Ganesan, N. Hanagata, *Adv. Healthcare Mater.* **2014**, *3*, 10.
[21] V. Švrček, A. Slaoui, J.-C. Muller, *J. Appl. Phys.* **2004**, *95*, 3158.
[22] D. Mariotti, V. Švrček, J. W. J. Hamilton, M. Schmidt, M. Kondo, *Adv. Funct. Mater.* **2012**, *22*, 954.
[23] V. Švrček, D. Mariotti, U. Cvelbar, G. Filipič, M. Lozac'h, C. McDonald, T. Tayagaki, K. Matsubara, *J. Phys. Chem. C* **2016**, *120*, 18822.
[24] V. Švrček, K. Dohnalova, D. Mariotti, M. T. Trinh, R. Limpens, S. Mitra, T. Gregorkiewicz, K. Matsubara, M. Kondo, *Adv. Funct. Mater.* **2013**, *23*, 6051.

[25] R. Guerra, E. Degoli, S. Ossicini, *Phys. Rev. B* **2009**, *80*, 155332.
[26] C. A. Schneider, W. S. Rasband, K. W. Eliceiri, *Nat. Methods* **2012**, *9*, 671.
[27] L. Pavesi, D. J. Lockwood, *Silicon Photonics*, Springer, Berlin, **2004**.
[28] A. A. Ischenko, G. V. Fetisov, L. A. Aslalnov, *Nanosilicon: Properties, Synthesis, Applications, Methods of Analysis and Control*, Taylor & Francis, London **2014**.
[29] P. Bertoncello, E. T. Kefalas, Z. Pikramenou, P. R. Unwin, R. J. Forster, *J. Phys. Chem. B* **2006**, *110*, 10063.
[30] M. S. Hybertsen, *Phys. Rev. Lett.* **1994**, *72*, 1514.
[31] P. Hapala, K. Kůsová, I. Pelant, P. Jelínek, *Phys. Rev. B* **2013**, *87*, 195420.
[32] J. P. Perdew, *Int. J. Quantum Chem.* **1985**, *28*, 497.
[33] A. J. Williamson, J. C. Grossman, R. Q. Hood, A. Puzder, G. Galli, *Phys. Rev. Lett.* **2002**, *89*, 196803.
[34] C. Delerue, M. Lannoo, G. Allan, *Phys. Rev. Lett.* **2000**, *84*, 2457.
[35] H.-Ch. Weissker, J. Furthmüller, F. Bechstedt, *Phys. Rev. B* **2002**, *65*, 155328.
[36] T. van Buuren, L. Dinh, L. Chase, W. Siekhaus, L. Terminello, *Phys. Rev. Lett.* **1998**, *80*, 3803.
[37] A. M. P. Botas, R. A. S. Ferreira, R. N. Pereira, R. J. Anthony, T. Moura, D. J. Rowe, U. R. Kortshagen, *J. Phys. Chem. C* **2014**, *118*, 10375.
[38] T. Lu, F. Chen, *J. Comput. Chem.* **2012**, *33*, 580.
[39] J. P. Perdew, K. Burke, M. Ernzerhof, *Phys. Rev. Lett.* **1996**, *77*, 3865.
[40] J. P. Perdew, K. Burke, M. Ernzerhof, *Phys. Rev. Lett.* **1997**, *78*, 1396.
[41] T. H. Dunning, P. J. Hay, *Methods of Electronic Structure Theory*, Vol. 3, Plenum Press, New York, **1977**.
[42] W. R. Wadt, P. J. Hay, *J. Chem. Phys.* **1985**, *82*, 284.
[43] C. E. Check, T. O. Faust, J. M. Bailey, B. J. Wright, T. M. Gilbert, L. S. Sunderlin, *J. Phys. Chem. A* **2001**, *105*, 8111.
[44] D. Feller, *J. Comput. Chem.* **1996**, *17*, 1571.
[45] K. L. Schuchardt, B. T. Didier, T. Elsethagen, L. Sun, V. Gurumoorthi, J. Chase, J. Li, T. L. Windus, *J. Chem. Inf. Model.* **2007**, *47*, 1045.
[46] TURBOMOLE6.4., TURBOMOLE GmbH, Karlsruhe, http://www.turbomole.com (accessed: April 2017).
[47] J. P. Perdew, M. Ernzerhof, K. Burke, *J. Chem. Phys.* **1996**, *105*, 9982.
[48] C. Adamo, V. Barone, *J. Chem. Phys.* **1999**, *110*, 6158.
[49] W. Ku, T. Berlijn, C.-C. Lee, *Phys. Rev. Lett.* **2010**, *104*, 216401.